Understanding the formation of ultrafine spinel CoFe2O4 nanoplatelets and their magnetic properties

Wenchao Liu, Yukkwan Chan, Jinzhu Cai, Chiwah Leung, Cheeleung Mak et al.

Citation: J. Appl. Phys. **112**, 104306 (2012); doi: 10.1063/1.4765033
View online: http://dx.doi.org/10.1063/1.4765033
View Table of Contents: http://jap.aip.org/resource/1/JAPIAU/v112/i10
Published by the AIP Publishing LLC.

Understanding the formation of ultrafine spinel CoFe2O4 nanoplatelets and their magnetic properties

Wenchao Liu,[1,a)] Yukkwan Chan,[2] Jinzhu Cai,[1] Chiwah Leung,[2] Cheeleung Mak,[2,a)] Kinhung Wong,[2] Fengming Zhang,[1] Xiaoshan Wu,[1] and X. D. Qi[3]
[1]*National Laboratory of Solid State Microstructures and Photovoltaic Engineering Center of School of Modern Engineering and Applied Sciences, Nanjing University, Nanjing 210093, China*
[2]*Department of Applied Physics and Materials Research Centre, The Hong Kong Polytechnic University, Hung Hom, Kowloon, Hong Kong SAR, China*
[3]*Department of Materials Science and Engineering, National Cheng Kung University, Tainan City 70101, Taiwan*

(Received 27 June 2012; accepted 12 October 2012; published online 21 November 2012)

Cobalt ferrite ($CoFe_2O_4$, CFO) nanoplatelets with a rhomboidal shape were synthesized through a facile hydrothermal route using a very low concentration precursor at low temperatures. The effects of reaction temperature and time on the morphologies as well as the sizes of the products were systemically investigated. The as-synthesized CFO nanocrystals showed a special rhomboidal shape with crystal growth along the (111) direction. The very low concentration precursor plays an important role in forming CFO nanocrystals with such special shape and ultrafine size. The single-phase CFO nanoplatelets synthesized at 180 °C with size of 17 nm present high saturation magnetization (79.7 emu/g) and high coercivity (3100 Oe). The preparation conditions have significant effects on the crystal size and shape, magnetization and relaxation activation of the CFO nanoplatelets. © *2012 American Institute of Physics*. [http://dx.doi.org/10.1063/1.4765033]

INTRODUCTION

Magnetic fine particles have potential applications in the field of biotechnology, data storage, environmental remediation and catalysis.[1–3] Spinal cobalt ferrite ($CoFe_2O_4$, CFO) is an outstanding magnetic material with high Curie temperature, large magneto-crystalline anisotropy, reasonable large magnetization, remarkable chemical stability and mechanical hardness.[4–6] Being a promising magnetic and electrical resistive material, CFO has attracted considerable attention for their applications as high density information storage device,[7] spintronic devices,[8,9] magnetoelectric transducers,[10,11] and actuators.[12,13] On the other hand, it is well-known that materials in nanoscale size range show significantly different physical and chemical properties as compared to their corresponding bulk solids. For example, CFO nanoparticle (above a certain size) is generally magnetic at room temperatures due to its large magneto-crystalline anisotropy and transition temperature, and thus is in great demand in various fields such as gas sensor and high density data storage. However, low-dimensional CFO crystal (~5 nm) with low energy barrier becomes superparamagnetic at room temperatures due to thermal fluctuations. This made them potential application in biomedicine field such as cell-separation and drug delivery.[14–17]

Considerable efforts have been spent on the synthesis of low-dimensional CFO including nanodots, nanorods, nanotubes, nanowires, and so on. Pham-Huu *et al.* synthesized CFO nanowires using the confinement effect concept provided by the carbon tubular morphology.[18,19] Similar, Ji *et al.* used anodic aluminum oxide (AAO) as templates to obtain CFO nanorods.[20] A particularly interesting work by Kinsella *et al.*[21] was to fabricate one-dimensional ordered CFO nanoparticles chains using DNA as sacrificial guiding molecule. Using this bottom-up DNA guide method instead of other conventional fabrication approaches, they obtained ordered CFO chains with very high aspect ratio (~10^3) that is in the range of several microns in length and less than 10 nm in diameter. Besides using template-based methods, some research groups[22,23] used a solution-based micelle method to synthesize one-dimensional CFO nanorods with the help of organic surfactants such as cetyltrimethylammonium bromide (CTAB). Apart from one-dimensional CFO, zero-dimensional CFO such as spherical and cubic nanocrystals, hollow spheres, microsphers and nanorings have been prepared in recent years.[24–29] Some groups reported that monodisperse CFO nanocrystals can be grown into a nearly spherical shape or an almost perfect cubic shape by using a seed-mediated growth approach. Indeed, the shape of the nanocrystals can be reversibly interchanged between spherical and cubic shape by controlling the nanocrystal growth rate.[24,25] Prozorov *et al.* developed a novel bioinspired synthesis route, employing a combination of bacterial mineralization proteins and hierarchically self-assembling polymers for synthesis of well-defined and shape-specific CFO nanocrystals. The as-synthesized nanoplatelets showed hexagonal shape with crystal growth along [111] direction, which are likely templated by the protein localized on hexagonally packed micelles.[30]

So far, most of these efforts devoted to the controlled synthesis of CFO nanostructures are based on wet chemistry synthesis, which relies on templates with either specific shape or organic molecules (surfactants, polymers, capping

[a)]Authors to whom correspondence should be addressed. Electronic addresses: wcliu@nju.edu.cn and apaclmak@polyu.edu.hk.

ligands, or bio-molecular) to manipulate the final sizes and shapes of the CFO nanocrystals. Herein, we introduce a high-yield synthesis of technologically important CFO nanocrystals with a rhomboidal shape, using a simplified hydrothermal method without the assistance of any surfactants or templates. The hydrothermal synthesis possesses remarkable reliability and selectivity as well as high efficiency at low temperature. It does not require any expensive precursors or equipment and can be readily adopted for industrial production processes. Although there were some studies on the synthesis of CFO nanocrystals by hydrothermal method in the last decade,[31–33] reports on CFO nanoplatelets syntheses with rhomboidal shape have not been found. We try to understand the initial formation process of the CFO crystals under the hydrothermal environment. We found that reaction temperature, reaction time and precursor concentration have great impact on the size and resultant morphology of the nanocrystals formed.

EXPERIMENTAL METHODS

Synthesis of $CoFe_2O_4$ nanocrystals

CFO spinel ferrite nanocrystals were synthesized by a hydrothermal method using a very low concentration precursor. The reagents $Co(CH_3COO)_2.4H_2O$ ($Co(ac)_2$, Aldrich) and $FeCl_3$ (Aldrich) with a molecular ratio of 1:2 were mixed to form an homogeneous aqueous solution. After stirring for 30 min, appropriate KOH were added into the solution and followed with another 30 min stirring to form the precursor. The final concentration of CFO precursor was fixed at 0.03 M. Then the precursor was transferred to a 50-ml Teflon-lined stainless autoclave, appropriate distilled water was put into it until 80% of its volume was filled. The mixture was sealed and allowed to heat at various temperatures (between 90 and 180 °C) for various time (between 3 and 24 h) under autogenous pressure. After cooling, the powders were centrifuged, washed with deionized water, ethanol and deionized water in sequence to remove the impurities and carbonate byproduct. The final product was dried in air at 60 °C overnight and weighted. The product yield was calculated to be 94%.

Characterization of $CoFe_2O_4$ nanocrystals

The CFO crystal structure of the samples was studied by a four-circle x-ray diffractometer (XRD, Philips X'pert Systems) with CuK_α ($\lambda = 0.154$ nm) radiation operated at an acceleration voltage of 50 kV. For the Fourier transform infrared spectroscopy (FTIR, NICOLET MAGNA-IR 760) investigation, the CFO nanocrystals were mixed with KBr powders and then pressed into semi-transparent pellets for measurements in transmission mode. Raman spectra were taken using 488 nm laser line of an air cooled Ar-ion laser. A microscope was used to focus the incident laser beam to a spot of about 100 μm in diameter. Raman spectra were recorded by a 100× lens system in back scattering geometry using a Horiba Jobin Yvon HR800 spectrometer with a charge-coupled device (CCD) detector. The size and shape of the obtained CFO nanocrystals were studied by the transmission electron microscopy (TEM, JEOL JEM2010), and from its selected area electron diffraction (SAED) and high resolution results, the crystal structure of the samples was further identified. Magnetic properties (M-H loop and temperature dependence of magnetization) of the CFO nanocrystals were characterized by a vibrating sample magnetometer (VSM, Lakeshore Model 7300 series). The AC susceptibility was investigated by a SQUID magnetometer (Quantum Design MPMS-5 S).

RESULTS AND DISCUSSION

XRD, FTIR, and Raman analysis

Figure 1 shows the XRD spectra of CFO nanocrystals obtained at different synthesized temperatures. The crystalline peaks (220), (311), (222), (400), (422), (511) and (440), indexed as cubic CFO ($Fd3m$, $a = 8.394$ Å), is consistent with the reported data (JCPDS File No. 22-1086, as shown in the bottom of Fig. 1). The XRD pattern indicates that the nanocrystals obtained via the current synthetic method has high phase purity. In fact, CFO is such a material which easily crystallizes under low hydrothermal temperature. We put the original precursor in the reaction vessel at room temperature for 24 h, and then washed the precursor by deionized water and ethanol and dried at room temperature for XRD. Surprisingly, two weak peaks corresponding to (311) and (440) were observed (Fig. 1(a)), indicating that part of the precursor materials were converted from amorphous to crystals. The broadness of the peaks exhibited the nanocrystalline nature of the sample. The observed peaks become sharper and stronger in intensity as the temperature increased from 120 to 180 °C. The average particle size of the nanoparticle was determined using the Scherrer formula,[34]

$$D = \frac{k\lambda}{\beta\cos\theta}. \quad (1)$$

Here k is a constant and equals to 0.89, β is the full-width at half maximum (FWHM) of the diffraction peak (400), λ is

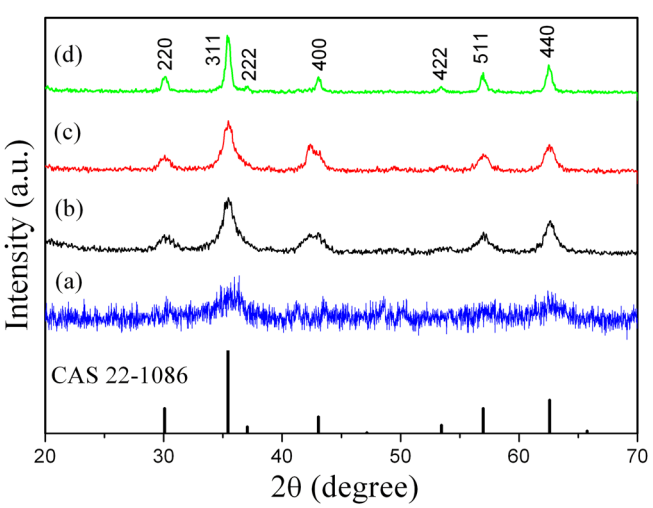

FIG. 1. XRD patterns of the CFO nanocrystals synthesized at (a) room temperature; (b) 120 °C; (c) 150 °C and (d) 180 °C. The bottom pattern is the standard of CFO from JCPDS File No. 22-1086.

the x-ray wavelength and θ is the Bragg angle. Since the peak of (311) is very close to (222) and this could induce some problems due to the overlap of the signals, we selected the diffraction peak (400) to calculate the size. The result is listed in Table I. The average crystallite size of CFO increases from 7.5 to 16.9 nm as synthesis temperature increases from 120 to 180 °C, respectively. This is well consistent with our TEM results.

In order to further monitor the CFO nanocrystals formation process, we use the FTIR to observe the change of chemical bonds of the CFO precursor during the hydrothermal synthesis process. Figure 2 shows the FTIR spectra of the CFO nanocrystals synthesized at various temperatures. The spectrum of CFO crystals synthesis at room temperature shows an absorption broad band at $\sim$3400 cm^{-1}, some absorption characteristic peaks at region of 1000 $\sim$ 1700 cm^{-1}, and a band at 600 cm^{-1}. The large absorption band centered at 3400 cm^{-1} can be assigned to the stretches of hydroxyl groups of gallery water molecules and hydrogen-bonded hydroxyl groups in cobalt and iron hydroxide.[35] The absorption band around 600 cm^{-1} is slightly larger than the typical value of metal oxide ($\sim$560 cm^{-1}) but smaller than that of metal hydroxide ($\sim$660 cm^{-1}).[36] Thus, it might be considered to be arisen from vibrations of mixture of O-Co-O, O-Fe-O and Co-OH, Fe-OH. This means, after hydrothermal treatment at room temperature, some cobalt and iron oxides were formed. This is consistent with the XRD result. Apart from these bands, two noticeable bands around 1515 and 1346 cm^{-1} were observed. We believe that these two bands are related to the intercalation of CH_3COO^- groups with cobalt hydroxide in the as-prepared precursor.[37] The peaks at 1515 and 1346 cm^{-1} with a frequency separation of 169 cm^{-1} can be attributed to the antisymmetric stretching and symmetric stretching vibrations of the free acetate ion ($-COO^-$), respectively.[38]

The FTIR spectra (Figs. 2(b) to 2(d)) of the spinel ferrites show two strong absorption bands in the range of 550 $\sim$ 600 cm^{-1}. Normally, the IR bands in the range of 300 $\sim$ 1000 cm^{-1} are assigned to the vibration of inorganic ions in the crystal lattice. These bands are assigned to the vibration of the metal ion-oxygen complexes in the tetrahedral and octahedral sites, respectively.[39] The existence of a band around the 560 cm^{-1} band strongly suggests the stretching of Me-O in tetrahedral sites, typical of the cobalt ferrite phase (γ_1 mode).[39] After hydrothermal treatment at above 120 °C, as shown in Fig. 2, most of the peaks assigned to –OH and -COO^- (at around 1000 $\sim$ 1700 cm^{-1}) disappear, and a new peak around 569 cm^{-1} assigned to the stretching mode of tetrahedral complexes in the spinel lattice occurs

TABLE I. Crystal size, H_c and M_s of CFO nanoparticles synthesized at different temperatures.

Temperature (°C)	120	150	180
XRD (nm)	7.5 ± 0.3	8.7 ± 0.3	16.9 ± 0.4
TEM (nm)	7.8 ± 0.4	9.0 ± 0.4	17.6 ± 0.6
H_c (Oe)	113 ± 2	353 ± 4	3100 ± 9
M_s (emu/g)	49.8 ± 2	68.8 ± 2	79.7 ± 3
M_r/M_s	0.12 ± 0.01	0.18 ± 0.01	0.54 ± 0.02

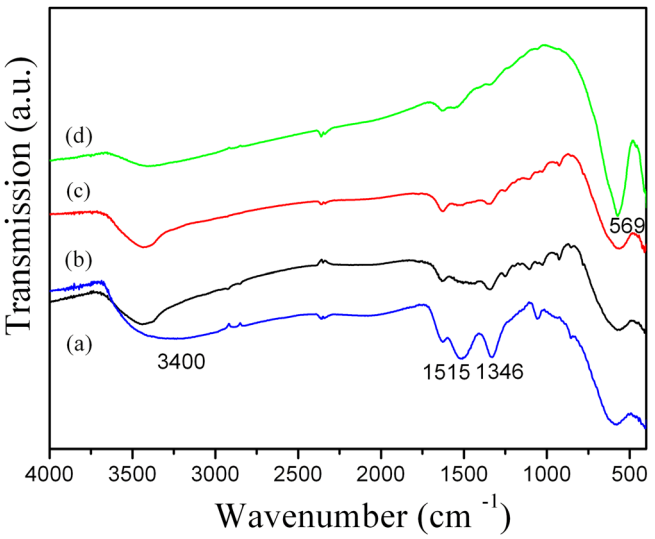

FIG. 2. FTIR spectra of the nanocrystals synthesized at (a) room temperature; (b) 120 °C; (c) 150 °C, and (d) 180 °C.

and the peaks become sharper with increasing temperature, which suggests that the CFO nanocrystals are basically formed and the nanocrystals synthesized at higher synthesis temperature show better crystalline quality.

Figure 3 shows the Raman spectra of the CFO nanocrystals synthesized at different temperatures. The spectrum of CFO ceramics synthesized by solid-state reaction method is also recorded and displayed for comparison. All the Raman bands are consistent with those reported for other cubic inverse spinel ferrite structures, which belong to the O_h^7 ($Fd\bar{3}m$) space group. The metallic cations occupy two types of positions: either surrounded by six oxygen ions to form an octahedron, or by four oxygen ions to form a tetrahedron. This spinel structure gives rise to 39 normal modes, among which 5 are Raman active.[40] The two Raman modes at around 461 cm^{-1} and 680 cm^{-1} are the characteristic modes of spinel ferrite: the low-frequency mode at 461 cm^{-1} is

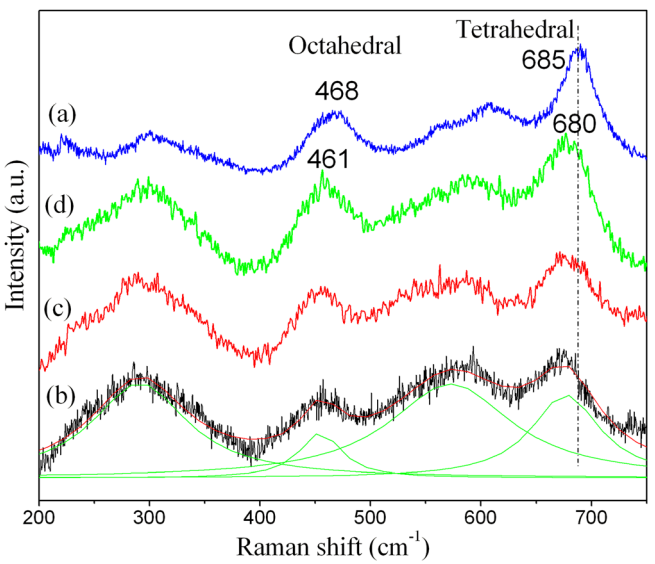

FIG. 3. Raman spectra of (a) bulk CFO and the CFO nanocrystals synthesized at (b) 120 °C; (c) 150 °C, and (d) 180 °C.

assigned as the vibrations of the octahedral sublattice, whereas the high energy phonon mode at 680 cm^{-1} originates from vibrations of the tetrahedral sublattice. On the other hand, it is important to note that the Raman peaks of the CFO nanocrystals are very broad and shift to low frequency as compared to that of the polycrystalline bulk ferrites; moreover, they broaden and soften as the nanocrystals size decreases. This feature is believed to be related to a consequence of phonon confinement effects in nanocrystals.[41]

The microstructure and morphology of the CFO nanocrystals were further examined using TEM, SAED and high resolution transmission electron microscopy (HRTEM), as shown in Fig. 4. The TEM micrograph in Fig. 4(a) reveals that though the sizes of the particles are not very uniform, all nanoplatelets synthesized at 180 °C show rhomboidal shape.

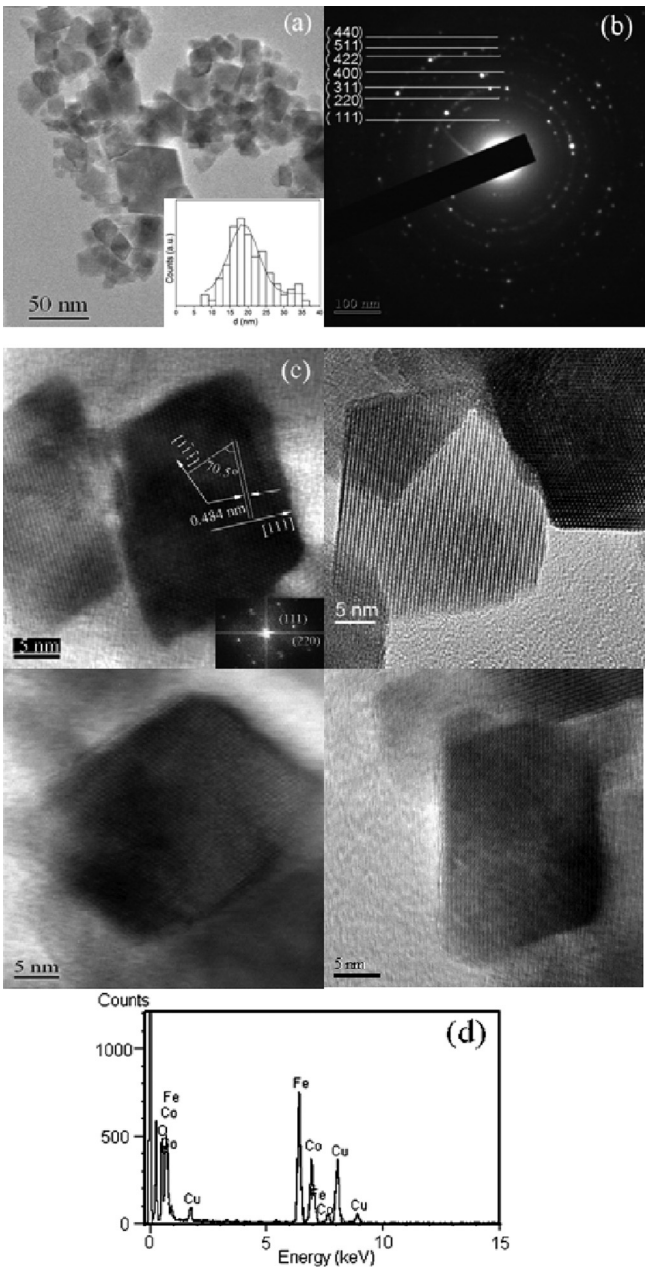

FIG. 4. (a) LRTEM (inset is distribution of particle size), (b) SAED, (c) HRTEM and (d) EDS of the CFO nanocrystals synthesized at 180 °C. The inset of part of (c) is the FFT pattern.

Figure 4(b) is a SAED acquired from the assembly of CFO nanoparticles. Figure 4(c) is the HRTEM image of a typical CFO nanocrystal and the corresponding lattice Fourier transform pattern (inset in Fig. 4(c)). In order to confirm the morphology of the CFO nanocrystals clearly, herein, we present four HR-TEM pictures of four different CFO nanocrystals. The diffraction rings were indexed as (111), (220), (311), (400), (422), (511) and (440), respectively, which is consistent with the XRD data. The HRTEM studies confirm that these nanoparticles are single crystals with no evidence of defects such as grain boundary, dislocation or stacking fault. Energy dispersive x-ray spectroscopic (EDS) analysis shows that there are elements of Fe, Co, and O in the sample (Fig. 4(d)), and the atom ratio of Co:Fe:O is 1:2.08:4.25, which is close to that of $CoFe_2O_4$ formula. All of the above analyses confirm that the synthesized sample is spinel CFO without any impurities.

Interestingly, in contrary to most published results where CFO powders presented spherical, cubic, rod-like or other shapes,[18–29] our synthesized CFO nanocrystals present a very regular rhomboidal platelets shape. The interplanar distance of the crystal fringes with an angle of 70.5° is 0.48 nm, which agrees well with the separation between the (111) lattice planes. What are the factors controlling such domain patterns and shapes? To address this issue, we consider the growth of a crystalline nucleus in hydrothermal conditions. In the early stages of nucleation and growth, the nucleus tends to grow in shapes dominated by surface energy terms. The surface energy anisotropy of spinels is different from that of perovskites such as $BaTiO_3$ and $SrTiO_3$.[42,43] Most perovskite phases are characterized by low-energy {100} surfaces and a corresponding equilibrium shape of a cube dominated by six {100} facets; in case of spinels, the {111} surface possesses low surface energy as compared to other surface,[44] as reflected in an equilibrium shape of an octahedron bounded by eight {111} facets.

Generally, 0-dimensional nanostructures tend to be circular due to their relatively low surface energy, but the CFO in this study developed into regular rhomboidal shape. In order to understand the possible morphological evolution mechanisms of the CFO nanocrystals with rhomboidal shapes, controlled experiments were conducted at 180 °C with various hydrothermal times. Figures 5(a) to 5(c) show a series of TEM images of CFO at different reaction stages corresponding to the reaction durations of 3, 12, and 24 hours, respectively, together with schematic illustration of the whole evolution process of the rhomboidal CFO nanocrystals. During the initial stage of the reaction (<3 h), the as-synthesized products consist of precipitates of hydroxides and amorphous nanoparticles caused by the incomplete reaction. The precursors subsequently self-assembled to grow and form CFO nanocrystals with an elongated plate morphology (Fig. 5(a)) after a prolonged reaction time of 3 h. The large particles grew at the expense of the smaller ones, driven by the tendency of the solid phase in the system to achieve a minimum total surface free energy. Upon extending the reaction time to 12 h, rhomboidal nanoplaletes grew out on these aggregated elongated plates (Fig. 5(b)). In the final stage of evolution (~24 h), most of the products were

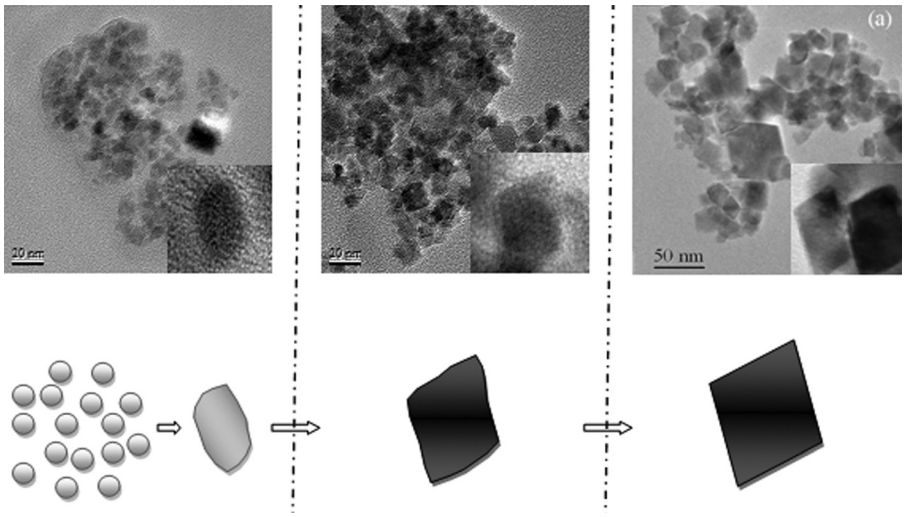

FIG. 5. TEM images of the products obtained from different reaction times of (a) 3 h (b) 12 h; and (c) 24 h; (d) Schematic illustration of the morphological evolution process for the rhomboidal CFO nanocrystals.

ready to evolve into regular rhomboidal shapes (Fig. 5(c)). It is believed that smoother crystal facets and bigger crystal size may be attained with a longer reaction time. Moreover, the concentration of the precursor in this experimental is very low, which plays an important role in the process of the nano CFO nuclear formation. We believe that it is helpful and feasible to investigate the initial stage of the CFO nuclear formation process using a very low concentration precursor. The formation of CFO nanoplatelets should be relevant to functionalized $Co(OH)_2$ as a soft structural template. In the precursor, the high concentration OH^{-1} gives a basic environment for the formation of cobalt hydroxide. A 2-dimensional sheet-like structure $Co(OH)_2$ forms as a general morphology due to its intrinsic lamellar structure, as reported by Yang *et.al*.[45] Under hydrothermal condition, the interlayers of 2-dimensional lamellar $Co(OH)_2$ micelles serve as microreactors and react with Fe^{3+} in the water to finally form CFO nanoplatelets in the interlayers. Here, we should notice that the low concentration precursor with low viscosity can slow the reaction speed and prohibit the aggregation of nanosheets to form bigger spatial structures.

Magnetic properties

Figure 6 shows the room temperature magnetization loops of CFO synthesized at different temperatures and synthesis duration. Hysteresis loops show that synthesized CFO nanocrystals depict ferromagnetic behavior. The inset of Fig. 6(b) shows photographs of CFO nanocrystals synthesized at 180 °C dispersed in ethanol without magnetic field and with magnetic field for 5 min. It proves that the as-synthesized CFO nanocrystal shows magnetic behavior and can be captured and easily separated by means of a simple magnet. As shown from TEM and XRD results, the crystal size increases with increasing synthesis temperature. Obviously, coercivity (H_c), saturation magnetization (M_s), remanent magnetization (M_r), and reduced remanent magnetization (Mr/Ms) show particle size dependency, that is, they all increase with increasing nanocrystal size, shown in Table I. The Ms value was obtained by fitting the high-field part of the hysteresis curve using the relation:[46]

$$M = M_s \times (1 - \frac{a}{H} - \frac{b}{H^2}), \quad (2)$$

Where H is the field strength, and a and b are parameters determined by the fitting procedure. It is noticed that M_s value of nanocrystals synthesized at 120 °C min is 49.8 emu/g, while for those prepared at 180 °C, the M_s increases dramatically to 79.7 emu/g corresponding to 98% of the reported bulk value (80.8 emu/g).[47] Normally the magnetization value of nano-sized crystals is influenced by two

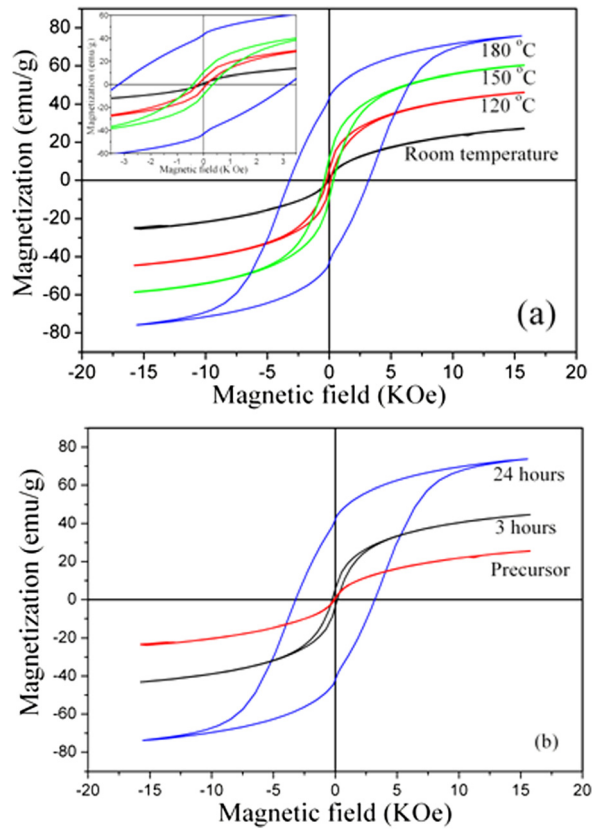

FIG. 6. Room temperature hysteresis loops of CFO nanoparticles synthesized at (a) different temperatures (The inset shows enlarged magnetic hysteresis loops at low applied fields); and (b) different time (at 180 °C) (The inset shows photographs of CFO nanocrystals dispersion in ethanol without magnetic field and with magnetic field for 5 min).

main factors, namely, the presence of parasitic phases and inversion degree. The existence of parasitic phases such as Fe_2O_3, Fe, Co, is eliminated by our XRD and Raman results. The spinel ferrite structure contains two interstitial sites, occupied by metal cations, with tetrahedral A-site and octahedral B-site. The cationic distribution in octahedral and tetrahedral sites may be quantified by the inversion degree, which can be defined as the fraction of divalent ions in the octahedral sites. The net magnetization is proportional to the difference between A and B sublattice magnetization, thus, the saturation magnetization depends on the cationic distribution (inversion degree). In nanostructured spinel ferrite material, the inversion degree is related surface spin-canting and finite size-effect. The reduction of saturation magnetization with the particle size is attributed to surface spin canting that yields magnetic disorder at the particle surface.[6,24,48] We also note that reduced remanent magnetization of CFO nanocrystals synthesized at 180 °C is around 0.5 at room temperature, indicating that these CFO particles possess uniaxial magnetic anisotropy. Note that reduced remanent magnetization decreases with the particle size, this is due to the change in magnetization reversal mode from coherent to incoherent rotation.[49] The reduced remanence of 180 °C synthesized nanocrystals is equal to 0.54 which is close to the theoretical value of 0.5 expected for noninteracting uniaxial single-domain particles with the easy axis randomly oriented. The reduction of saturation magnetization of nanocrystals synthesized at 180 °C is much larger than those of 120 and 150 °C synthesized samples due to the enhancement of the effective anisotropy.[50]

The H_c refers to the amount of external magnetic field required to reduce the overall magnetization of the sample to zero, after the sample has reached magnetic saturation. The coercivity varies from 114 to 3100 Oe as the crystal size increase from 7 to 18 nm. Generally the magnetization reversal mechanism includes magnetization vector rotation in mono-domain crystals and domain wall motion in multi-domain crystals. The critical size of a mono-domain CFO particle is estimated to be 40 nm,[51] which is far larger than the average diameter of our CFO nanocrystals. So the obtained magnetic CFO nanoparticles possess single magnetic domain. In single domain magnetic nanoparticles, the particles become spontaneously magnetized with net ordered magnetic moments pointed to some preferred direction when the temperature is below Curie or Néel magnetic temperature. The preferred direction usually is some certain crystallographic axis associated with the magneto-crystalline anisotropy energy (E_A). The correlation between E_A and the volume of the nanocrystal V can be expressed by the Stoner-Wohlfarth theory,[52]

$$E_A = KV\mathrm{Sin}^2\theta, \tag{3}$$

where K is the magneto-crystalline anisotropy constant, and θ is the angle between the easy axis and the magnetization direction. This anisotropy serves as the energy barrier to prevent the change of magnetization direction. Therefore, bigger particles would result in a larger E_A, and a higher magnetic field is needed to change the moment direction, resulting in higher value of H_c.

Figure 7 shows the temperature dependence of the magnetization of the CFO synthesized at 180 °C. With increasing temperature, a large drop in magnetization occurred. This indicates a sharp ferromagnetic to paramagnetic transition, and the Curie temperature T_c derived by the peak of $dM(T)/dT$ (as shown in the inset of Fig. 7) is 787 K, which is close to that of the bulk (792 ~ 798 K).[53]

For nano-sized magnetic mono-crystals, we are also interested in their superparamagnetic behavior at room temperature; in such a state, the magnetic order still exists in the nanoparticles, with each particle behaves like a paramagnet but with a giant magnetic moment. When a superparamagnetic state is achieved, the magnetic nanoparticle goes through a superparamagnetic relaxation process, in which the magnetization direction of the nanoparticle fluctuates instead of being fixed along certain direction, yielding a zero net magnetization. The blocking temperature T_B is defined as the temperature at which the magnetic anisotropy energy barrier of a nanoparticle is overcome by thermal activation and becomes superparamagnetic relaxed. As shown in Fig. 6, all CFO nanocrystals synthesized above 120 °C show ferrimagnetic behavior at room temperature. If the size is further decreased, the CFO nanocrystals will present superparamagnetic behavior at room temperature. Thus, we further lowered the synthesized temperature to 90 °C to get smaller CFO nanocrystals (~5 nm). Figure 8(a) shows the zero-field-cooled (ZFC) and FC results measured in the field of 1.5 K Oe. It is found that the ZFC curve gradually deviates from the FC curve at temperatures below 170 K. Thus, we obtained the blocking temperature, T_B, of about 170 K. The inset of Fig. 8(a) shows the M-H loop measured at 300 K and 5 K respectively. It is obvious that the CFO nanocrystals synthesized at 90 °C shows superparamagnetic properties at nearly room temperature. Meanwhile, this ultrafine nanocrystals have a reduced remanence Mr/Ms of 0.42 at 5 K which is close to theoretical value of 0.5 for noninteracting uniaxial single-domain particles with the easy axis randomly oriented.[54,55]

Understanding and controlling the superparamagnetic properties of nanocrystals is crucial to many important

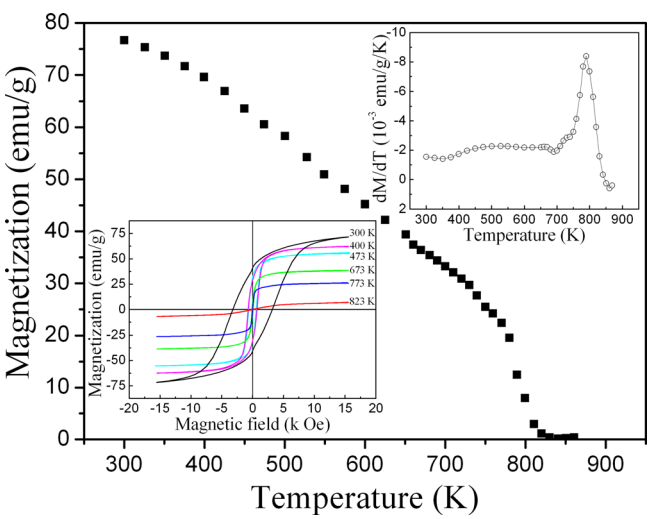

FIG. 7. Temperature dependence of the magnetization of the CFO nanocrystals synthesized at 180 °C. The left inset is the hysteresis at various temperatures. The right inset is the relationship of dM/dT vs T.

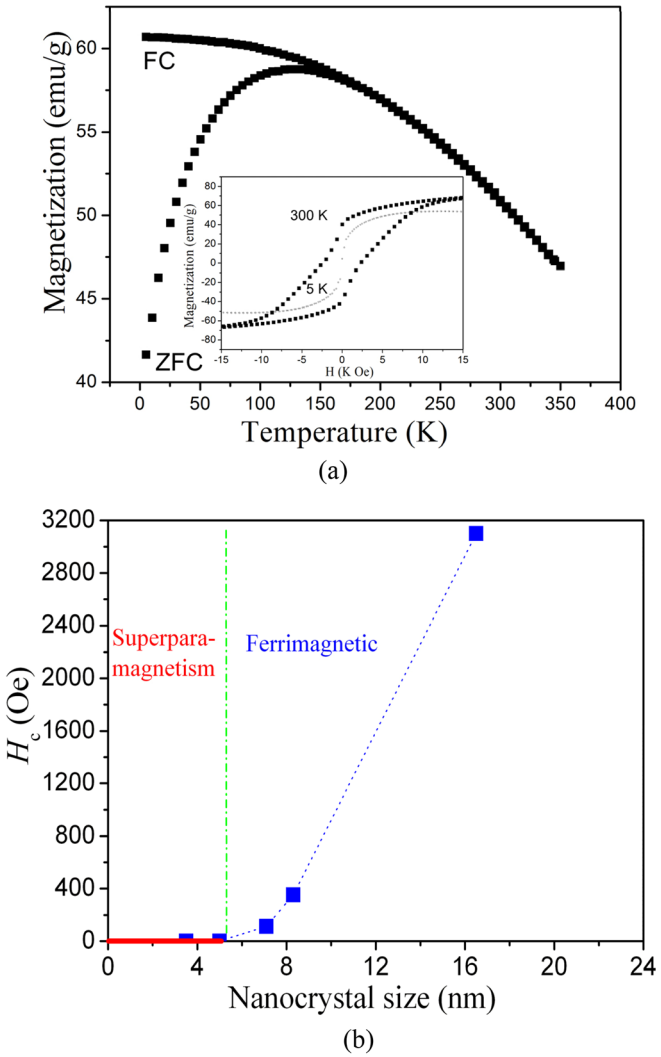

FIG. 8. (a) Temperature dependence of the magnetization of CFO nanocrystals synthesized at 90 °C obtained in ZFC/FC process with applied field of 1.5 K Oe. The inset shows the M-H hysteresis loops at 5 K and 300 K. (b) The relationship between H_c and crystal size.

applications. For instance, to pursue high-density information storage, the size of magnetic bits should be further reduced. However, in order to keep the digital data usable, the superparamagnetic relaxation of the magnetization direction in the data bits should be avoided. On the other hand, superparamagnetic relaxation is an essential requirement for the magnetic nanoparticles used as magnetic resonance imaging, cell-separation and drug delivery. All of these can be achieved through controlling the size and magnetic anisotropy (shape) of CFO nanocrystals by changing the synthesis temperature and duration (Fig. 8(b)).

CONCLUSIONS

In summary, a facile hydrothermal method was developed to synthesize spinel CFO nanoplatelets with a regular rhomboidal shape. This method allows the size and shape control with high yield, where both size and shape are two very important aspects for practical applications. The morphological evolution process for the rhomboidal CFO nanoplatelets was discussed through investigating the morphology of nanocrystals synthesized with different durations by TEM. The ultra low surface energy of {111} facet of spinels is believed to be responsible for the formation of the special rhomboidal shape. The single-phase CFO nanoplatelets synthesized at 180 °C with size of 17 nm present high saturation magnetization (79.7 emu/g) and high coercivity (3100 Oe). The CFO nanocrystals synthesized above 120 °C show a ferrimagnetic behavior while the CFO nanocrystals synthesized at 90 °C present a superparamagnetic behavior. The ability to design the nanoparticles with or without superparamagnetic properties over a large size range certainly facilitates the applications of magnetic nanocrystals for high-density data storage, DNA separation and drug delivery using nanoparticulate magnetic carriers.

ACKNOWLEDGMENTS

This work was supported by the National Natural Science Foundation of China (51202108, 10974081, 10979017, 11274153) and NKPBRC (2010CB923404). Dr. Liu thanks the support from a research grant from the Hong Kong Polytechnic University (Grant No. J-BB9Q).

[1]J. L. Dormann, D. Fiorani, and E. Tronc, *Magneticrelaxation in Fine-Particlessystems*, Adv. in Chem. Physics Vol. XCVIII (New York, 1997).
[2]S. Morup, M. F. Hansen, and C. Frandsen, *Magnetic Nanoparticle* (Elsevier, 2011).
[3]G. C. Papaefthymiou, Nano Today **4**, 438 (2009).
[4]D. Peddis, C. Cannas, G. Piccaluga, E. Agostinelli, and D. Fiorani, Nanotechnology **21**, 125705 (2010).
[5]R. Comes, H. Liu, M. Khokhlov, R. Kasica, J. Lu, and S. A. Wolf, Nano Lett. **12**, 2367 (2012).
[6]D. Peddis, N. Yaacoub, M. Ferretti, A. Martinelli, G. Piccaluga, A. Musinu, C. Cannas, G. Navarra, J. M. Greneche, and D. Fiorani, J. Phys.: Condens. Matter. **23**, 426004 (2011).
[7]E. Snoeck, C. Gatel, R. Serra, G. BenAssayag, J. B. Moussy, A. M. Bataille, M. Pannetier, and M. Gautier-Soyer, Phys. Rev. B **73**, 104434 (2006).
[8]M. J. Carey, S. Maat, P. Rice, R. F. C. Farrow, R. F. Marks, A. Kellock, P. Nguyen, and B. A. Gurney, Appl. Phys. Lett. **81**, 1044 (2002).
[9]K. Inomata, N. Ikeda, N. Tezuka, R. Goto, S. Sugimoto, M. Wojcik, and E. Jedryka, Sci. Technol. Adv. Mater. **9**, 014101 (2008).
[10]H. Zheng, J. Wang, S. E. Lofland, Z. Ma, L. Mohaddes-Ardabili, T. Zhao, L. Salamanca-Riba, S. R. Shinde, S. B. Ogale, F. Bai, D. Viehland, Y. Jia, D. G. Schlom, M. Wuttig, A. Roytburd, and R. Ramesh, Science **303**, 661 (2004).
[11]K. Srinivas, G. Prasad, T. Bhimasankaram, and S. V. Suryanarayana, Mod. Phys. Lett. B **14**, 663 (2000).
[12]S. Monz, A. Tschope, and R. Birringer, Phys. Rev. E **78**, 021404 (2008).
[13]F. Gazeau, C. Baravian, J. C. Bacri, R. Perzynski, and M. I. Shliomis, Phys. Rev. E **56**, 614–618 (1997).
[14]X. F. Chu, D. L. Jiang, G. Yu, and C. M. Zheng, Sens. Actuators B **120**, 177 (2006).
[15]L. Loo, R. H. Guenther, S. A. Lommel, and S. Franzen, J. Am. Chem. Soc. **129**, 11111 (2007).
[16]R. Colognato, A. Bonelli, D. Bonacchi, G. Baldi, and L. Migliore, Nanotoxicology **1**, 301 (2007).
[17]D. H. Kim, D. E. Nikles, D. T. Johnson, and C. S. Brazel, J. Magn. Magn. Mater. **320**, 2390 (2008).
[18]C. Pham-Huu, N. Keller, C. Estournes, G. Ehret, J. M. Greneche, and M. J. Ledoux, Phys. Chem. Chem. Phys. **5**, 3716 (2003).
[19]C. Pham-Huu, N. Keller, C. Estournes, G. Ehret, and M. J. Ledoux, Chem. Commun. **2002**, 1882 (2002).
[20]G. B. Ji, S. L. Tang, B. L. Xu, B. X. Gu, and Y. W. Du, Chem. Phys. Lett. **379**, 484 (2003).
[21]M. Kinsella and A. Ivanisevic, J. Phys. Chem. C. **112**, 3191 (2008).
[22]Z. T. Zhang, A. J. Rondinone, J. X. Ma, J. Shen, and S. Dai, Adv. Mater. **17**, 1415 (2005).

[23]G. B. Ji, S. L. Tang, S. K. Ren, F. M. Zhang, B. X. Gu, and Y. W. Du, J. Cryst. Growth **270**, 156 (2004).
[24]O. Song and Z. J. Zhang, J. Am. Chem. Soc. **126**, 6164 (2004).
[25]N. Z. Bao, L. M. Shen, P. Padhan, and A. Gupta, Appl. Phys. Lett. **92**, 173101 (2008).
[26]Z. M. Li, X. Y. Lai, H. Wang, D. Mao, C. J. Xing, and D. Wang, J. Phys. Chem. C. **113**, 2792 (2009).
[27]Y. D. Meng, D. R. Chen, and X. L. Jiao, Eur. J. Inorg. Chem. **2008**, 4019 (2008).
[28]C. Cannas, A. Ardu, A. Musinu, D. Peddis, and G. Piccaluga, Chem. Mater. **20**, 6364 (2008).
[29]H. Zhang, C. X. Zhai, J. B. Wu, X. Y. Ma, and D. R. Yang, Chem. Commun. **2008**, 5648 (2008).
[30]T. Prozorov, P. Palo, L. Wang, M. Nilsen-Hamilton, D. Jones, D. Orr, S. K. Mallapragada, B. Narasimhan, P. C. Canfield, and R. Prozorov, ACS Nano **1**, 228 (2007).
[31]D. Zhao, X. Wu, H. Guan, and E. Han, J. Supercrit. Fluids **42**, 226 (2007).
[32]S. Komarneni, M. C. D'Arrigo, C. Leonelli, G. C. Pellacani, and H. Katsuki, J. Am. Ceram. Soc. **81**, 3041 (1998).
[33]X. H. Li, C. L. Xu, X. H. Han, L. Qiao, T. Wang, and F. S. Li, Nanoscale Res. Lett. **5**, 1039 (2010).
[34]W. C. Liu, D. Wu, A. D. Li, H. Q. Ling, Y. F. Tang, and N. B. Ming, Appl. Surf. Sci. **191**, 181 (2002).
[35]J. M. Fernandez, C. Barriga, M. A. Ulibarri, F. M. Labajos, and V. Rives, J. Mater. Chem. **4**, 1117 (1994).
[36]L. N. Zhang, M. F. Zhou, L. M. Shao, W. N. Wang, K. N. Fan, and Q. Z. Qin, J. Phys. Chem. A. **105**, 6998 (2001).
[37]Y. C. Zhu, H. L. Li, Y. Koltypin, and A. Gedanken, J. Mater. Chem. **12**, 729–733 (2002).
[38]S. Doeuff, M. Henry, C. Sanchez, and J. Livage, J. Non-Cryst. Solids **89**, 206 (1987).
[39]G. V. S. Rao, C. N. R. Rao, and J. R. Ferraro, Appl. Spectrosc. **24**, 436 (1970).
[40]T. Yu, Z. X. Shen, Y. Shi, and J. Ding, J. Phys.: Condens. Matter **14**, L613 (2002).
[41]Z. V. Popovic, Z. Dohcevic-Mitrovic, M. Scepanovic, M. Grujic-Brojcin, and S. Askrabic, Ann. Phys. **523**, 62 (2011).
[42]J. Padilla and D. Vanderbilt, Phys. Rev. B. **56**, 1625 (1997).
[43]T. Sano, D. M. Saylor, and G. S. Rohrer, J. Am. Ceram. Soc. **86**, 1933 (2003).
[44]R. K. Mishra and G. Thomas, J. Appl. Phys. **48**, 4576 (1977).
[45]L.-X. Yang, Y.-J. Zhu, L. Li, L. Zhang, H. Tong, W.-W. Wang, G.-F. Cheng, and J.-F. Zhu, Eur. J. Inorg. Chem. **2006**, 4787 (2006).
[46]C. Cannas, A. Musinu, G. Piccaluga, D. Fiorani, D. Peddis, H. K. Rasmussen, and S. Mørup, J. Chem. Phys. **125**, 164714 (2006).
[47]M. Grigorova, H. J. Blythe, V. Blaskov, V. Rusanov, V. Petkov, V. Masheva, D. Nihtianova, L. M. Martinez, J. S. Munoz, and M. Mikhov, J. Magn. Magn. Mater. **183**, 163 (1998).
[48]R. H. Kodama, A. E. Berkowitz, E. J. McNiff, and S. Foner, Phys. Rev. Lett. **77**, 394 (1996).
[49]T. Ibusuki, S. Kojima, O. Kitakami, and Y. Shimada, IEEE Trans. Magn. **37**, 2223 (2001).
[50]L. D. Tung, V. Kolesnichenko, D. Caruntu, N. H. Chou, C. J. O'Connor, and L. Spinu, J. Appl. Phys. **93**, 7486 (2003).
[51]C. N. Chinnasamy, B. Jeyadevan, K. Shinoda, K. Tohji, D. J. Djayaprawira, M. Takahashi, R. J. Joseyphus, and A. Narayanasamy, Appl. Phys. Lett. **83**, 2862 (2003).
[52]E. C. Stoner and E. P. Wohlfarth, IEEE Trans. Magn. **27**, 3475 (1991).
[53]G.A. Sawatsky, F. Van Der Woude, A. H. Morrish, J. Appl. Phys. **39**, 1204 (1968).
[54]E. C. Stoner and E. P. Wohlfarth, Philos. Trans. R. Soc. London, Ser. A **240**, 599 (1948).
[55]D. Peddis, M. V. Mansilla, S. Mørup, C. Cannas, A. Musinu, G. Piccaluga, F. Orazio, F. Lucari, and D. Fiorani, J. Phys. Chem. B. **112**, 8507 (2008).